

Quantum Interference in Deformed Carbon Nanotube Waveguides

WeiFa^{1,2} and Jinming Dong¹

¹ National Laboratory of Solid State Microstructures and Department of Physics, Nanjing University, Nanjing, 210093, People's Republic of China

² Department of Applied Physics, Nanjing University of Aeronautics and Astronautics, Nanjing, 210016, People's Republic of China

Abstract

Quantum interference (QI) in two types of deformed carbon nanotubes (CNTs), i.e., axially stretched and AFM tip-deformed CNTs, has been investigated by the π -electron only and four-orbital tight-binding (TB) method. It is found that the rapid conductance oscillation (RCO) period is very sensitive to the applied strains, and decreases in an inverse proportion to the deformation degree, which could be used as a powerful experimental tool to detect precisely the deformation degree of the deformed CNTs. Also, the coupling effect is found to be negligible under axially stretched strain, while it works on the transport properties of the tip-deformed CNTs.

PACS numbers: 62.25.+g, 73.22.-f, 73.63.Fg

The mechanical and electronic properties of carbon nanotubes (CNTs) have drawn a great deal of interests due to the potential applications in developing further quantum devices.¹⁻³ A perfect CNT can act as either a metal or a semiconductor, depending on its helicity and diameter.^{4,5} However, various mechanical deformations may exist in the actual CNTs due to their experimental surroundings, which can bring substantial changes of their electronic structures.⁶⁻⁸ For examples, a metal-semiconductor transition occurs under uniaxial strain for all metallic CNTs except arm chair ones, and the change rate of band gap vs strain increases as the chiral angle decreases. Additionally, the conductance of a metallic CNT could decrease by several orders of magnitude under the manipulation of an atomic force microscope (AFM) tip, presenting a possible application of the CNTs in nano-engineering, such as nanoscale sensors and electromechanical switches, on the basis of the controllable fabrications of the deformed CNTs. Though intensive studies have been carried out to understand the deformed CNTs, there still exist many experimental and theoretical uncertainties about the intimate relationships between their electrical and mechanical properties. Also, how to measure the deformation degree remains a major challenge to the existing experimental techniques.

It is well-known that the quantum interference (QI) between electron waves becomes increasingly crucial as electronic devices shrink down to nanometer size.⁹⁻¹¹ The rapid and slow conductance oscillations (RCO and SCO) of the metallic CNT electron resonators have been observed to be dependent on the tube length and chiral angles.^{12,13} Jiang et al. have derived an analytical expression and successfully explained the above experimental results, showing that both the RCO and SCO are induced by the intrinsic QI.¹⁴ However, the effects of deformation have not been considered in their work. Just as the optical interference plays an important role in modern precise measurements, the QI of electron waves may be also useful in detecting precisely nano-size structures.

Therefore, in this paper, we first present our numerical simulations on two types of deformed CNTs, i.e. axially stretched and AFM-deformed CNTs. We find that the hybridization effect is negligible on the electronic properties of the axially stretched CNTs, but works on those AFM-deformed CNTs. The most interesting finding is that the RCO period decreases as the increase of deformation in both cases, which may provide a powerful experimental tool to measure precisely the deformation degree of the deformed CNTs.

The whole model system consists of a central CNT and two semi-infinite leads (left and

right), which, for simplicity, are taken to be the same tubes as the central sample. We have studied two kinds of different chiral CNTs in detail, which, for comparison, the original length of the central sample (L) is taken to be approximately equal, containing 146 unit cells for the arm chair tube (6, 6) and 84 cells for the zigzag one (12, 0), respectively. For simplicity, we label the $(n;m)$ CNT with k cells as $(n;m)_k$ throughout the paper.

Atomic simulations are carried out on our samples by considering two types of deformation, i.e., stretched tubes under uniform uniaxial strain and tubes pushed by an atomically sharp AFM tip. To simulate the former, the tube is firstly stretched rigidly by a distance L along its axis with one side fixed. Then, atoms at both sides of the central sample, contacting with the leads, are fixed and the remaining structure is relaxed with the universal force field (UFF).¹⁵ As shown in Fig. 1, for the tip deformation, a 15-atom Li-needle normal to the (100) direction is chosen to model the AFM tip as in Ref. 8, which is first aimed at the center of a hexagon on the bottom side of the middle part and then pushed downward vertically by a displacement L to bend the CNT, resulting in the total length of the deformed tube to be $L + \sqrt{L^2 + 4L^2}$. The whole injected tube is then relaxed by UFF, keeping the needle atoms and the end atoms of both sides fixed. Since the external stress is locally concentrated in the middle part adjacent to the Li-tip, a structural optimization based on density functional theory (DFT) is further applied to relax a smaller 240-atom section in the middle. The DFT code used here is Acelrys' DMol3,¹⁶ in which the electronic wave functions are expanded in a double-numerical polarized (DNP) basis set with a real-space cutoff of 4.0 Å. Approximation used in the Hamiltonian is the Harris functional¹⁷ with a local exchange-correlation potential.¹⁸ The injected tube at every deformation degree is relaxed sufficiently, and so a quasi-static process is simulated.

To compare the two types of deformation directly, we denote the deformation degree by the tube-length change. For example, the 5% strain means a total tube-length increase of 5 percent, either in axially stretched or tip-induced deformation. The cross section holds a nearly perfect circle in the stretched CNT with bonds almost uniformly elongated along the tube-axis. In contrast, there exists a more increase of the average bond length in the highly deformed region of the tip-deformed tube. It is interesting that, as those discussed in Ref. 8, sp^2 -coordinated configurations are kept in the action of tip, even for the largest deformation (10%) considered here.

Then, the quantum conductance fluctuation of the deformed CNT electron resonator

has been calculated by the tight-binding (TB) model including only the nearest-neighbor interactions. Firstly, we use a simple π -electron approximation, in which all the hopping integrals are assumed to be $V_{pp} = 2.75 \text{ eV}$ ¹⁹ multiplied by a scaling factor $(r_0/r_i)^2$, where r_0 and r_i are bond lengths without and with deformation, respectively.²⁰ In order to simulate the boundary effect, for those atoms at contacts, their hopping parameters are taken to be V_p with $0 < \alpha < 1$. Consequently, electrons will be slightly scattered at the interfaces for $\alpha \neq 1$ and the whole system behaves like a Fabry-Perot electron waveguide, whose conductance G is calculated by the Landauer formula $G = \frac{2e^2}{h}T$, where T is the transmission coefficient. Since the transmission probability T reaches to 0.5–0.95, as shown in the experiment,¹³ the α value is reasonably set to be 0.7 in our simulations.²¹

Four-orbital calculations are also performed to show the σ -coupling effect. The hopping integrals are taken to be close to those used for graphite,²² i.e., $V_{ss} = 4.43 \text{ eV}$, $V_{sp} = 4.98 \text{ eV}$, $V_{pp} = 6.38 \text{ eV}$, and $V_{pp} = 2.66 \text{ eV}$, which have been successfully used in the SWNT with small radius.²³ Among the four orbitals per atom, its s level is located at $\epsilon_s^0 = -7.3 \text{ eV}$ below the triply-degenerated p level taken as the zero of energy. Like the π -electron calculations, the same bond-length-dependence of the nearest-neighbor hopping parameters is taken into account.

The results obtained by using a single π -orbital are discussed firstly. We calculate conductance of two perfect-CNT electron resonators, which will be used as benchmarks for analyzing the QI of the deformed tubes. Obtained results as a function of Fermi Energy are shown in Fig. 2, from which the general characteristics can be clearly found. Both of the CNT electron resonators, (6;6)146 and (12;0)84, display remarkable RCO with their maximum conductance approaching $2G_0$, but a SCO background is present obviously in the armchair tube and absent for the zigzag one. As interpreted in Ref. 14, both the RCO and SCO are the QI phenomena, which come from the linear and nonlinear terms in the energy dispersion relations, respectively. The zigzag CNT resonator has no SCO due to existence of identical energy dispersion relations for its two propagating modes. The calculated RCO period ΔE_F equals to 51.54 meV for (6, 6)146 and 52.12 meV for (12, 0)84, which agree very well with the theoretical prediction $\Delta E_F = \hbar v_F/2L = 18.3926/L$ (L is the tube-length in unit of Å). In addition, a small band gap exists in the zigzag tube (12, 0) due to curvature, induced by the bond-dependent hopping integrals.

Then, we consider effects of the two types of deformation on the conductance oscillations

and the corresponding results are illustrated in Figs. 3 and 4. For clarity, we just show the cases of deformed tubes with length increases of 5% and 10% in Fig. 3. Application of uniaxial strain opens a band gap only for the zigzag tube, which is coincident with the conclusion of Ref. 6. Of special interest is that both the RCO and SCO are preserved well for the stretched CNTs up to axial strain of 10%. Moreover, it is obvious that the RCO period decreases with increase of deformation, which is illustrated by its frequency shift to the higher one, shown in the inset of Fig. 3. For example, the RCO periods of the (6, 6)146 under strain of 5% and 10% equal to 48:10 meV and 44:50 meV, respectively. For the axially stretched zigzag tube, though the band gap is opened, the successive decrease of the RCO period is still distinct, since the overall stretching causes the change of the phase difference. It can be seen obviously from Fig. 3 that the RCO becomes faster near the band edges of the stretched (12, 0) tube, in which a higher frequency with smaller amplitude emerges in the frequency analysis except the intrinsic RCO frequency. Additionally, obtained results of the two achiral tubes show that the change rate of the RCO period with respect to strain ($d(E_F)/d(\text{strain})$) may be also chirality-dependent (see Fig. 4).

As for the AFM tip-deformed tubes, the situation becomes more complicated. Although the arm chair tube (6, 6) remains metallic under all conditions considered, there exists a large drop in its conductance around E_F when the total-length increase exceeds 7% due to existence of localized states induced by the concentrated local strain in the middle part. However, the RCO and SCO of the arm chair tubes are still obvious in the tip deformation and the decrease of the RCO period is also observed, as illustrated in Fig. 3 (a). For the tip-deformed zigzag tube (12, 0), the main characteristics of QI are similar to those in the stretched strain. Interestingly, a new fluctuation with a half of the RCO frequency appears more obviously with increase of tip-deformed degree, which may be induced by the heavy local structural deformation near tip and ascribed to nonlinear effects. By plotting E_F versus tip-deformed degree in Fig. 4, we found that the slope of $d(E_F)/d(\text{strain})$ is slightly larger than that of the axially stretched deformation. This is not surprising because a larger tensile strain exists in the middle of the tip-deformed tube, while the increase of bond-length is almost uniform in the axially stretched CNT.

It is clearly seen from Fig. 4 that both of our numerical results on the axially stretched and tip-deformed CNTs are almost quantitatively consistent with those from the analytical formula in Ref. 14. However, there is still a minor difference between them, especially for

the larger strains (e.g. $> 3\%$), caused by a non-uniform change of the bond lengths in the present finite-length CNTs. That is to say, both the total tube-length and the bond-length changes can affect the RCO.

Furthermore, four-orbital TB calculations are performed to take into account any effect associated with π -hybridization. For axially stretched deformation, the main results about the RCO period agree with the π -orbital results presented in Figs. 3 and 4: the RCO period change is inversely proportional to the deformation degree. The difference is that the slope of $d(E_F)/d(\text{strain})$ is slightly steeper than that of the π -orbital results, which means the effect of the stretched bond-length on E_F is more distinct due to π -hybridization.

However, the π -coupling has actual effects on the transport properties of the tip-deformed CNTs. Taking the tip-deformed (6, 6)146 as an example, as illustrated in Fig. 5, the SCO can survive in the case of smaller tip-deformation ($< 6\%$), but will be smeared out as the strain becomes larger. Additionally, it is also seen from Fig. 5 that the localized states have more important influence on the system conductance than the corresponding π -orbital results. For example, the concentrated local strain induces a conductance dip above E_F for 5% strain, in which a localized state at 0.68 eV appears. However, though the SCO gradually disappears with increase of the tip-deformation degree, the RCOs still keep in every case. More importantly, the E_F decreases gradually as the tip pushes, and the main frequency shifts to a higher one. As a result of the stretched tube-length, the RCO period does decrease with increase of deformation degree in both cases, i.e. the axial strain and tip-induced deformation.

In addition, we have also calculated other finite-length tubes with different chiralities, such as (8, 2)55 and (6, 3)32, and found that chiral tubes satisfying $n - m = 3$ integer have similar results as those of the (12, 0)84. Thus we can conclude that our conclusions obtained above are suitable for the QI of the metallic deformed-CNT electron resonators.

In conclusion, we have shown that the two types of mechanical deformations can significantly modify the QI of CNTs and the RCO periods are very sensitive to the applied strains. It is found that although there are some differences in the QI of the two types of deformed CNTs, the RCO period change depends mainly on the tube-length and is inversely proportional to the strain. Since the Fermi energy change E_F is driven by the gate voltage V_g as $E_F = C_{\text{eff}} V_g$ (typically, the gate efficiency factor $C_{\text{eff}} = 0.01 - 0.05$), a measurement of the RCO can offer a possible powerful tool to measure precisely the deformation

degree of the deformed CNT. Application of such techniques may therefore open a door in future to use a metallic CNT as a tiny electro-mechanical switch under the effects of various deformations.

This work was supported by the Natural Science Foundation of China under Grants Nos. A040108 and 90103038.

-
- ¹ H. Dai, E. W. Wong, and C. M. Lieber, *Science* 272, 523 (1996).
 - ² T. W. Tombler, C. Zhou, L. Alexseyev, J. Kong, H. Dai, L. Liu, C. S. Jayanthi, M. Tang, and S. Wu, *Nature (London)* 405, 769 (2000).
 - ³ E. D. Miot, Y. Yaish, V. Sazonova, J. Y. Park, M. Brink, and P. L. McEuen, *Phys. Rev. Lett.* 90, 156401 (2003).
 - ⁴ N. Hamada, S. I. Sawada, and A. Oshiyama, *Phys. Rev. Lett.* 68, 1579 (1992).
 - ⁵ T. W. Odom, J. L. Huang, P. Kim, and C. M. Lieber, *Nature (London)* 391, 62 (1998).
 - ⁶ L. Yang and J. Han, *Phys. Rev. Lett.* 85, 154 (2000).
 - ⁷ L. Liu, C. S. Jayanthi, M. Tang, S. Y. Wu, T. W. Tombler, C. Zhou, L. Alexseyev, J. Kong, and H. Dai, *Phys. Rev. Lett.* 84, 4950 (2000).
 - ⁸ A. Maiti, A. Svizhenko, and M. P. Anantram, *Phys. Rev. Lett.* 88, 126805 (2002).
 - ⁹ H. C. Manoharan, C. P. Lutz, and D. M. Eigler, *Nature (London)* 403, 512 (2000).
 - ¹⁰ Y. Ji, M. Heiblum, D. Sprinzak, D. Mahalu, and H. Shtrikman, *Science* 290, 779 (2000).
 - ¹¹ P. Deybray, O. E. Raichev, P. Vasilopoulos, M. Rahman, R. Perrin, and W. C. Mitchell, *Phys. Rev. B* 61, 10950 (2000).
 - ¹² W. Liang, M. Bockrath, D. Bozovic, J. H. Hafner, M. Tinkham, and H. Park, *Nature (London)* 411, 665 (2001).
 - ¹³ J. Kong, E. Yenilmez, T. W. Tombler, W. Kim, H. Dai, R. B. Laughlin, L. Liu, C. S. Jayanthi, and S. Y. Wu, *Phys. Rev. Lett.* 87, 106801 (2001).
 - ¹⁴ J. Jiang, J. Dong, and D. Y. Xing, *Phys. Rev. Lett.* 91, 56802 (2003).
 - ¹⁵ A. K. Rappe, C. J. Casewit, K. S. Colwell, W. A. Goddard, and W. M. Skiff, *J. Am. Chem. Soc.* 114, 10024 (1992).
 - ¹⁶ B. Delley, *J. Chem. Phys.* 92, 508 (1990); *J. Phys. Chem.* 100, 6107 (1996);
<http://www.accelrys.com/mstudio/dm ol3.htm>

- ¹⁷ J. Harris, Phys. Rev. B 31, 1770 (1985). If a more realistic simulation is performed, a charge transfer between the CNT and the Li tip maybe exists, giving only a disturbance on the conductance oscillations, which, however, can be remedied by the applied gate voltage.
- ¹⁸ S. H. Vosko, L. W.ilk, and M. Nusair, Can. J. Phys. 58, 1200 (1980).
- ¹⁹ L. Chico, V. H. Crespi, L. X. Benedict, S. G. Louie, and M. L. Cohen, Phys. Rev. Lett. 76, 971 (1996).
- ²⁰ W. A. Harrison, Electronic Structure and the Properties of Solids (Dover, New York, 1989).
- ²¹ The conductance oscillations appear at the strong coupling between the electrical contact and the CNT, and become well-defined resonant peaks as the coupling is very weak. [L. Yang, J. Chen, H. Yang, and J. Dong, Phys. Rev. B 69, 153407 (2004).
- ²² D. Tomaneek and S. G. Louie, Phys. Rev. B 37, 8327 (1988)
- ²³ X. Blase, L. X. Benedict, E. L. Shirley, and S. G. Louie, Phys. Rev. Lett. 72, 1878 (1994).

Figure Captions

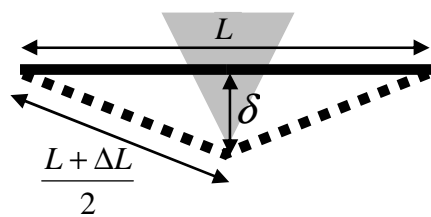
FIG .1. The CNT indented by an AFM tip. (a) Schematic view; (b) Relaxed structure of the tip-deformed tube (12, 0) with a length increase of 7 percent, shown only 240 atoms in the middle (further relaxed by DFT). The Li tip (white balls) and ending atoms (black balls) are fixed at their respective classical positions in the DFT optimization.

FIG .2. TB π -electron results on conductance G (in unit of G_0) vs Fermi energy E_F with $\gamma = 0.7$ for perfect CNTs: (a) (6, 6)146 and (b) (12, 0)84.

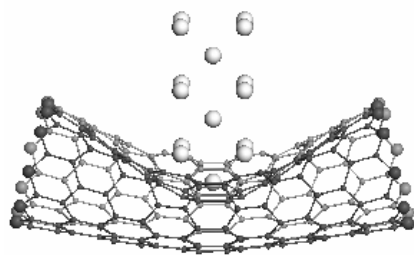
FIG .3. TB π -electron results on conductance G vs Fermi energy E_F with $\gamma = 0.7$ for the deformed tube: (a) (6, 6)146 and (b) (12, 0)84. For clarity, only 5% and 10% strain are shown for the axially stretched and tip-induced deformation, denoted by $\backslash S$ and $\backslash Tip$ ", respectively. The inset in each panel is the corresponding frequency analysis for the conductance oscillation, in which the dotted line represents the oscillation frequency of the perfect tube.

FIG .4. (Color online) RCO period change of the deformed tubes, obtained from a TB π -electron calculation. The dashed line corresponds to the analytical result for the axially stretched tube (6, 6)146.

FIG .5. Four-orbital TB results for the perfect (6, 6)146 and its tip-deformed cases under strain of 5% and 10%. The left panel gives the conductance G vs Fermi energy E_F with $\gamma = 0.7$, and the right panel shows the corresponding frequency analyses. For comparison, the π -electron frequency analyses are also shown by the dashed lines.



(a)



(b)

